

Article

Borate and Silicate Bioactive Glass Coatings Prepared by Nanosecond Pulsed Laser Deposition

Julietta V. Rau ^{1,2,*}, Angela De Bonis ^{3,*}, Mariangela Curcio ³, Katharina Schuhlade ⁴,
Katia Barbaro ⁵, Giovanni De Bellis ^{6,7}, Roberto Teghil ³ and Aldo R. Boccaccini ⁴

¹ Istituto di Struttura della Materia, Consiglio Nazionale delle Ricerche (ISM-CNR),
Via del Fosso del Cavaliere, 100-00133 Rome, Italy

² Department of Analytical, Physical and Colloid Chemistry, Institute of Pharmacy, Sechenov First Moscow
State Medical University, Trubetskaya 8, build. 2, 119991 Moscow, Russia

³ Dipartimento di Scienze, Università della Basilicata, Via dell'Ateneo Lucano, 10-85100 Potenza, Italy;
mariangela.curcio@unibas.it (M.C.); roberto.teghil@unibas.it (R.T.)

⁴ Department of Materials Science and Engineering, Institute of Biomaterials, University of
Erlangen-Nuremberg, Cauerstr.6, 91058 Erlangen, Germany; katharina.ks.schuhlade@fau.de (K.S.);
aldo.boccaccini@ww.uni-erlangen.de (A.R.B.)

⁵ Istituto Zooprofilattico Sperimentale Lazio e Toscana "M. Aleandri", Via Appia Nuova,
1411-00178 Rome, Italy; katia.barbaro@izslt.it

⁶ DIAEE-Department of Astronautical, Electrical and Energy Engineering, Sapienza University of Rome,
via Eudossiana 18, 00184 Rome, Italy; giovanni.debellis@uniroma1.it

⁷ CNIS-Research Centre on Nanotechnology Applied to Engineering, P.le Aldo Moro 5, 00185 Rome, Italy

* Correspondence: giulietta.rau@ism.cnr.it (J.V.R.); angela.debonis@unibas.it (A.D.B.)

Received: 26 October 2020; Accepted: 16 November 2020; Published: 18 November 2020



Abstract: Silicate (13-93) and borate (13-93-B3) bioactive glass coatings were successfully deposited on titanium using the nanosecond Pulsed Laser Deposition technique. The coatings' microstructural characteristics, compositions and morphologies were examined by a number of physico-chemical techniques. The deposited coatings retain the same functional groups of the targets, are a few microns thick, amorphous, compact and crack free. Their surface is characterized by the presence of micrometric and nanometric particles. The surface topography, investigated by Atomic Force Microscopy, is characterized by spherical or ellipsoidal particles of the 0.2–3 μm size range for the 13-93 silicate bioactive glass film and of the 0.1–1 μm range for the 13-93-B3 borate bioactive glass coating. Equine adipose tissue-derived mesenchymal stem cells (ADMSCs) were applied for biological tests and the osteogenic differentiation activity of cells on the deposited coatings was studied after ADMSCs growth in osteogenic medium and staining with Alizarin Red. Cytocompatibility and osteogenic differentiation tests have shown that thin films retain the biocompatibility properties of the target silicate and borate glass, respectively. On the other hand, no antibacterial activity of the borate glass films was observed, suggesting that ion doping is advisable to inhibit bacterial growth on the surface of borate glass thin films.

Keywords: borate bioactive glass coatings; silicate bioactive glass coatings; nanosecond pulsed laser deposition; equine adipose tissue-derived stem cells; cytocompatibility; antibacterial activity

1. Introduction

Biomedical researchers are increasingly paying attention to the development and application of bioactive materials. In particular, in the field of prosthetic dentistry, maxillofacial surgery and orthopaedics, bioactive glasses and ceramics are increasingly chosen with respect to bioinert materials. In the 1960s, the first generation of biomaterials was selected for biomedical use due to their

suitable physico-chemical characteristics and inertness in biological environments [1]. From the 1980s, bioactive materials with a controlled interaction with the biological surroundings were preferred for clinical use [1,2]. Nowadays, bioactive materials belonging to the third generation are being developed with the aim to induce a desired therapeutic effect [1].

Among bioinert materials, titanium (Ti) is still widely used to manufacture hard-tissue implants, especially for load-bearing application (hip, knee and dental prosthesis), due to its optimal mechanical characteristics. It has been employed for orthopedic implants since the 1960s, when Brånemark and his co-workers [3] discovered a titanium cage strongly integrated in a rabbit bone a few months after its implantation. However, it is not osteogenic; therefore, the osteointegration takes place over a longer time, during which the eventual occurrence of shift movements between the implant and the host bone could lead to the formation of a fibrous capsule around the implant surface and its consequent failure may occur. In order to increase the chances of successful bone-related implant procedures, the modification of the Ti surface by coating it with a bioactive material is advisable [4–9]. In this way the optimal bulk mechanical properties are preserved, and the implant surface is more suitable to provide a better osteointegration.

After Hench's discovery of the 45S5 Bioglass® in 1971 [10], significant progress was made in bioactive glass composition, which aimed to design biomaterials possessing specific properties for bone reconstruction. The goal was to obtain materials whose components, dissolved in the extracellular matrix, are able to stimulate specific biological responses, influencing gene expression, osteogenic differentiation and cellular proliferation. In addition, the risk of infection incurrence after a surgery is always high and more probable in the case of implantation [11]. A way to prevent microbial colonization and the consequent implant failure is to impart antimicrobial properties to biomaterials.

Moreover, in order to overcome problems related to phase separation [10,12,13] and devitrification during heat treatment of early silicate glasses, other ions were added to their composition. In particular, the addition of components such as potassium, magnesium, and boron improved glass processability, making it easier to produce glass without crystallization and to use it in the form of coating, fibers, scaffolds, etc. [13]. For this purpose, Brink and co-workers carried out a systematic study on the *in vivo* bone-bonding behavior of several glass compositions [13,14]. Among these, the glass registered as 13-93 ($\text{Na}_2\text{O}-\text{K}_2\text{O}-\text{MgO}-\text{CaO}-\text{P}_2\text{O}_5-\text{SiO}_2$) had bioactive properties and was approved by the Food and Drug Administration in the USA and Europe for *in vivo* use. However, similarly to 45S5, the 13-93 bioactive glass is characterized by a slow and incomplete conversion into hydroxyapatite (HA) once in contact with the body fluids. For this reason, silicate was substituted by different percentages of borate, observing a faster and a more complete transformation into HA in the absence of silica [15–19]. This is because when borate glass is placed in the biological environment, there is no formation of a silica-rich layer, typical of the interaction process of the silicate glasses. Therefore, the reaction rate is limited by the dissolution of ions in biological surroundings [15–18,20,21].

Furthermore, boron has a number of key functions inside the biological environment, especially in bone metabolism, thanks to its interaction with calcium, magnesium and vitamin D, and, therefore, its presence is even more crucial for bone preservation and osteoporosis limitation [22,23]. Some studies evidenced that boron influences osteogenic differentiation of mesenchymal stem cells [24,25], being also angiogenic [26]. Many studies report that ion doping enhances the antibacterial properties of borate based bioglass [27–30]. On the other hand, Fu and collaborators [31] observed no beneficial effect on cell proliferation during *in vitro* testing, supposing an overly fast boron release in culture medium, while no toxic effects were found during *in vivo* testing due to the more dynamic microenvironment of the organism, which allows a rapid metabolization of boron. All these advantages make borate glasses a valuable alternative to conventional silicate bioactive glasses.

The potential of bioactive glass to be used as coating materials for metallic or alloy implants is related to the possibility of obtaining coating films that are dense, without cracks and well adherent to the substrate. Many of the coatings' techniques require high temperature treatment in order to allow the glass to react with the substrate surface [32–34]. In this contest, borate glasses are advantageous

with respect to silicate ones since boron oxide reduces the coefficient of thermal expansion of glass, better matching the coefficient of thermal expansion of metal substrate [29].

Among several deposition techniques, pulsed laser deposition is a promising route to obtain thin films for biomedical applications. The use of pulsed laser deposition (PLD) has in fact several advantages: coatings usually retain the bulk target composition, strongly adhere to the substrate surface, their thickness and crystallinity can be controlled by monitoring deposition parameters and their morphologies are typically characterized by nanometric and micrometric features [4,6,8,35], which support the osteointegration process [8,36,37]. Moreover, no heating treatment is required to deposit amorphous films.

Recently, several bioactive glasses [9,38–40] have been successfully deposited by PLD. Ma et al. [38] obtained, by PLD, Magnesium-containing bioactive glass coatings on Ti–6Al–4V that demonstrated higher corrosion resistance with respect to the uncoated substrates and film bioactivity by *in vitro* assay. Sanz et al. [39] deposited Niobium-containing bioactive glass on Ti substrate by nanosecond PLD, obtaining typical compact and granular films, which preserved target stoichiometry and improved cell adhesion in comparison with non-coated Ti. Rau et al. [6] coated Ti substrate with Cu-releasing bioactive glasses by nanosecond-PLD, showing their good wettability, bioactivity and antibacterial properties upon *in vitro* assay. Shaikh et al. [40] laser deposited 45S5 glass on Ti-alloy surface, testing films' biocompatibility on U2OS human osteosarcoma cells. Wang et al. [41,42] obtained composite hydroxyapatite/bioglass films by depositing, with a pulsed laser, on Ti–6Al–4V titanium alloy and demonstrated their osteoconductivity after implantation in shin bone of a rabbit.

In the present work, for the first time, borate-based (13-93-B3) and silicate-based (13-93) bioactive glasses (BGs) were deposited on titanium surface by nanosecond PLD at room temperature. The amorphous deposited films are compact and without cracks. Their surface presents nanometric and micrometric features that make films suitable for interaction with the biological medium. The coatings' biological properties were tested on equine adipose tissue-derived mesenchymal stem cells (ADMSCs) and microbiological tests were carried out, showing that borate-based glasses can be used as alternative materials to silicate glasses for the coating of titanium implants.

2. Materials and Methods

Silicate (13-93) and borate glasses (13-93-B3) were used as target materials for the pulsed laser deposition procedure.

2.1. Glasses Preparation

Silicate 13-93 (5.5 Na₂O, 11.1 K₂O, 4.6 MgO, 18.5 CaO, 3.7 P₂O₅, 56.6 SiO₂, all in wt.%) and borate 13-93-B3 (5.5 Na₂O, 11.1 K₂O, 4.6 MgO, 18.5 CaO, 3.7 P₂O₅, 56.6 B₂O₃, all in wt.%) glasses were prepared by a melt-quenching method, reported in [18]. Briefly, the synthesis was carried out in a platinum crucible using all analytical grade reagents (Na₂CO₃, K₂CO₃, MgO, CaCO₃, CaHPO₄·2H₂O, H₃BO₃) from Sigma-Aldrich (Steinheim, Germany), while the silicate source was a Belgian quartz sand (obtained from Åbo Akademi, Finland). The mixtures were heated for 2 h at 1050 °C and for 3 h at 1360 °C to obtain 13-93-B3 and 13-93 glasses, respectively. Afterwards, the melts were cast, annealed and crushed. The melting process was repeated twice. Bioactive glass blocks were crushed using a jaw crusher and milled using a planetary mill (both made of zirconia, Retsch, Haan, Germany). The obtained bioactive glass powders (0.3 g per pellet, with a mean particle size of 5–20 µm) were pressed into pellets (diameter of 10 and 3 mm height) using a hydraulic press (PE-010, MautheMaschinenbau, Wesel, Germany) with a load of 1t. The pressed pellets were then sintered at 1050 °C for 2 h with a heating rate of 2 °C per min.

Prior to depositions, the target materials were characterized by X-ray diffraction (XRD), by means of a D5000 (Siemens AG, Munich, Germany) in a θ – 2θ configuration, and by Fourier-transform infrared (FT-IR) spectroscopy, with a JASCO 460 Plus (Tokyo, Japan).

2.2. Pulsed Laser Deposition

The 13-93 and 13-93-B3 bioactive glass films were deposited on Si (100) and Ti 1 cm × 1 cm (both from Goodfellows, Huntingdon, UK) substrates. Ti substrates were preliminarily sandblasted and polished with a HNO₃/H₂SO₄ solution (aqua regia). Film depositions were performed in a stainless steel vacuum chamber equipped with a rotating target holder, at a pressure of 10⁻⁴ Pa. The Nd:YAG laser (Handy YAG, Quanta System, Samarate, Italy) with the following characteristics was used: λ = 532 nm, pulse duration = 7 ns, repetition rate = 10 Hz. It was directed on the target by quartz lens (45°, 350 mm focal plane). In each deposition, the target-substrate distance was kept at 2 cm, the deposition time was 5 h and the laser fluence was 12 J/cm²; such experimental conditions were optimized in our previous work [4].

2.3. Characterization

The composition of the films deposited onto Si substrates was characterized by FT-IR (JASCO 460 Plus), in transmittance mode in the range of 4000–400 cm⁻¹, by collecting 100 scans with a resolution of 4 cm⁻¹. This analysis was carried out on the films deposited onto Si (100) substrates since silicon shows very weak absorption in medium IR range. The crystalline or amorphous character of the films were investigated by XRD (D5000). The morphology was characterized by scanning electron microscopy (SEM) (PHILIPS-FEI XL30, North Billerica, MA, USA), while the roughness was evaluated by atomic force microscopy (AFM). AFM measurements were carried out by a Bruker Dimension Icon system (Billerica, MA, USA), equipped with a Nanoscope V controller (Bruker Corporation, Billerica, MA, USA). AFM micrographs were acquired in tapping mode, by using n-doped Si probes (Bruker RTESP300, Billerica, MA, USA) with a resonant frequency of roughly 300 kHz, at a scan rate between 0.3 and 1 Hz. Scanned areas ranged from 1 μm × 1 μm to 10 μm × 10 μm. At least three different regions were scanned for each sample. The roughness coefficients are presented as average values.

2.4. Biological Test

2.4.1. Equine Adipose Tissue-Derived Mesenchymal Stem Cell (ADMSC): Isolation and Culture

Adipose tissue was collected from a 2 year-old male horse. It was stored at 4 °C in a sterile container with phosphate buffer saline (PBS, from Sigma-Aldrich, Irvine, UK), supplemented with 5% *v/v* penicillin-streptomycin. After a quick transportation in laboratory, it was washed three times with PBS in order to remove red blood cells, dissected in small pieces and digested at 37 °C for 60 min with 0.1% collagenase Type IA (Sigma-Aldrich, Saint Louis, MO, USA). After that, cell suspension was centrifuged at 800 rpm for 10 min. The obtained pellet was re-suspended in the Dulbecco's Modified Eagle's Medium (DMEM) with 10% (*v/v*) fetal bovine serum (FBS, Gibco, Paisley, UK) and cultured in polystyrene flasks for cell cultures (Falcon, Durham, NC, USA). For this purpose, an incubator kept at 37 °C with a humidified atmosphere containing 5% of CO₂ was used. After 24 h culture medium, cellular debris were removed by washing with PBS. Culture medium (DMEM with 10% FBS) was added and then changed every two days until a cell confluence of 80% was reached. Subsequently, ADMSCs were trypsinized (with trypsin from Sigma-Aldrich, London, UK) and re-suspended in fresh culture medium.

2.4.2. Cell Viability

In order to investigate the effect of the 13-93 and 13-93-B3 coated Ti on the viability of the ADMSC cells, the 3-[4,5-dimethylthiazole-2-yl]-2,5-diphenyltetrazolium bromide (MTT) assay was performed. The MTT assay is a colorimetric test used to evaluate the cellular metabolic activity. It is based on the enzymatic reduction of MTT to water insoluble formazan blue salts, determinable spectrophotometrically. This reaction can occur only in viable cells due to the presence of mitochondrial succinate dehydrogenase (SDH).

ADMSCs with a concentration of 50,000 cells/mL in culture medium (DMEM with 10% FBS) were distributed in 24-well plate and incubated for 24 h at 37 °C. After that, the 13-93 and 13-93-B3 coated Ti samples were introduced and incubated under the same conditions. Before cell culture, the samples were washed with distilled water and sterilized in autoclave (121 °C, 20 min, pressure of 1.1 bar). The MTT assay was carried out after 24 and 48 h of incubation, when culture medium was substituted by the MTT solution (Sigma-Aldrich, London, UK) 0.5 mg/mL in the DMEM. After an incubation time of 3 h under cell culture conditions, the MTT solution was substituted with isopropanol (Sigma-Aldrich) and left for 30 min at room temperature, in order to dissolve formazan crystals, detected by measuring the optical density (OD) at 600 nm with a BioPhotometer (Eppendorf, Hamburg, Germany). All experiments were made in triplicate.

2.4.3. Osteogenic Differentiation

ADMSCs (50,000 cells/mL) were seeded in a 12-well plate (Falcon) and incubated under cell culture conditions (37 °C, 5% CO₂). After 24 h, the 13-93 and 13-93-B3 coated Ti and control samples without coatings were added, and the osteogenic differentiation was induced by changing the culture medium with an osteogenic one, composed of ascorbic acid 50 µg/mL (Sigma-Aldrich), β-glycerophosphate 10 mM (Sigma-Aldrich) and dexamethasone 10⁻⁷M (Sigma-Aldrich) in the DMEM plus 10% FBS, and incubated under cell culture conditions for three weeks, changing the culture medium every two days. ADMSCs in DMEM plus 10% FBS with and without osteogenic medium were positive and negative controls, respectively.

The osteogenic differentiation was evaluated by staining with Alizarin Red S (Sigma-Aldrich), which allows the detection of calcified extracellular matrix deposits, forming bright-red complexes with calcium. The images were taken by the means of an inverted optical microscope (Nikon, Eclipse TE 2000U, Tokyo, Japan).

2.4.4. Antibacterial Studies

The antibacterial activity was evaluated against *Enterococcus faecalis* (*E. faecalis*), *Escherichia coli* (*E. coli*), *Pseudomonas aeruginosa* (*P. aeruginosa*) and *Staphylococcus aureus* (*S. aureus*). All the bacteria strains were grown in Brain Heart Infusion (BHI, DIFCO, Sparks, NV, USA) in the presence of the sterilized 13-93 and 13-93-B3 coated Ti for 24 h at 37 °C. Bacterial growth was evaluated by measuring the optical density (OD_{600 nm}) by means of a BioPhotometer (EppendorfD30, Hamburg, Germany). Samples with OD values over the measurement range were appropriately diluted. All experiments were made in triplicate.

2.5. Statistical Analysis

All the experiments were carried out in triplicate and the results are expressed as mean ± standard deviation (SD). Statistical analysis was performed using the Origin Pro 9.0 software (Originlab Corporation, Northampton, MA, USA) and one-way ANOVA (Analysis of Variance) was applied, followed by a post hoc Tukey test. Values of $p < 0.05$ were considered statistically significant, indicated by an asterisk (*).

3. Results and Discussion

3.1. Physico-Chemical Characterization

Based on the results obtained by the FT-IR analysis of films deposited on the Si substrates, it is possible to conclude that the deposited coatings maintain the spectral figures of targets (Figure 1). The main absorption band of the 13-93 silicate glass target and film (Figure 1a) in the 1100–900 cm⁻¹ range is related to the Si–O–Si stretching mode. In particular, in the target it is possible to distinguish between the stretching mode Si–O–(with non-bridging oxygen), around 930 cm⁻¹, and the symmetric stretching mode of Si–O–Si, around 1020 cm⁻¹. Signals related to the bending and the asymmetric

stretching of Si–O–Si are also visible in the target and film spectra at 470 and 760 cm^{-1} , respectively. In the FT-IR spectra of both the target and of the film (Figure 1b) of the 13-93-B3 borate glass, the bending vibration of borates is observable at 715 cm^{-1} , whereas the bands centered at 1000 and 1400 cm^{-1} are related to the B–O stretching mode of BO_4 units (tetrahedral coordinated) and BO_3 (trigonal coordinated) units, respectively. The presence of different structural units is due to the ability of boron to transform its coordination number with oxygen in a borate glass network due to the presence of metal oxides, as in this case, that promotes the change from 3-fold to 4-fold coordination [43].

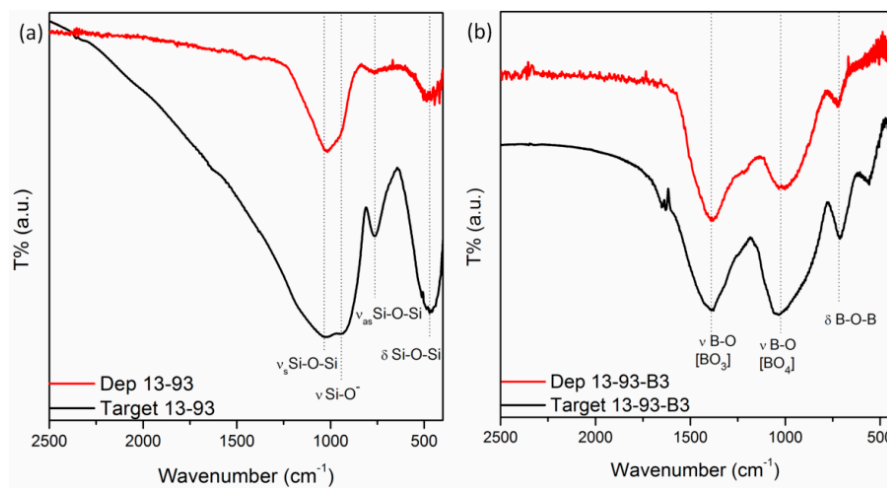


Figure 1. FT-IR spectra of target materials (black lines) and deposited films (red lines) of (a) 13-93 and (b) 13-93-B3 BGs.

It can be observed from the broad XRD patterns without any detectable peaks shown in Figure 2 that both of the target materials are amorphous with no measurable amount of crystalline phase [18]. The 13-93 glass spectrum presents a broad peak in the 25° – 30° region that is typical for silicate glass [18]. In the 13-93-B3 spectrum, a broad peak appears, centered at about 45° , that can be related to the borate content of the glass. To obtain crystalline films, nanosecond PLD deposition is usually performed by the heating of the substrate or by using a buffer gas [41,44,45], so we can expect that also the deposited films are amorphous. We deposited the films at room temperature since it was demonstrated that amorphous materials show superior solubility in biological or simulated biological fluid media and are characterized by an increased bioactivity with respect to crystalline materials [8,9,29,46].

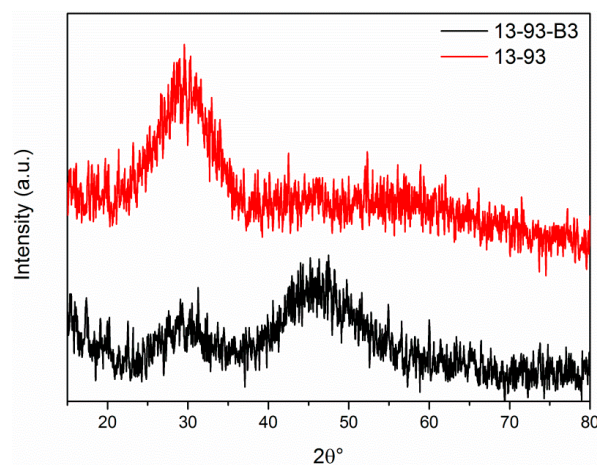


Figure 2. XRD patterns of 13-93 and 13-93-B3 BG targets material and deposited films.

The morphologies, registered by SEM (Figure 3), of films obtained by depositing silicate or borate targets are very similar. The films are uniform, dense, compact and without cracks. Micrometric particles homogeneously spread all over the surface and nanometric particles embedded in the dense background (Figure 3b,d) can be observed. Elongated and top flat microparticles are present on the surface of both films. The observed morphology is typical for ceramic films deposited by nanosecond PLD [4,6,8,35,39], where two different mechanisms of film growth are present: gas condensation and nano and micrometric droplets' coalescence. Gas condensation leads to the formation of the dense background covered by micrometric fused particles. Film surfaces, characterized by nanometric and micrometric features, may contribute to the implant's osteointegration [36,37].

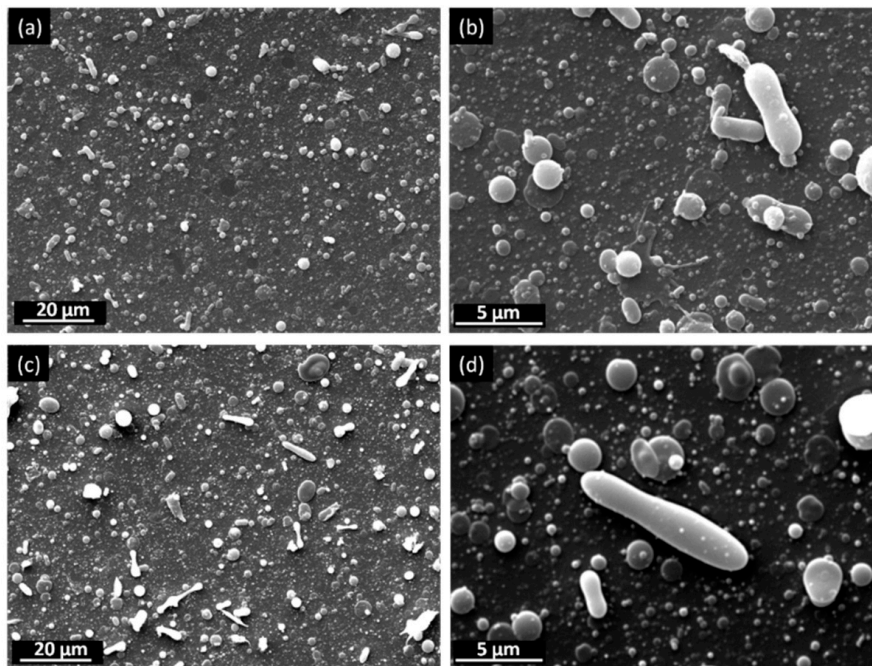


Figure 3. SEM images of (a,b) 13-93 and (c,d) 13-93-B3 BG coated Ti, registered at two different magnifications.

When a biomaterial is introduced into a living organism, the biochemical process responsible for osteointegration starts with the ion dissolution. During all the steps that lead to the formation of the apatite layer on the top of the implant, dynamic absorption and desorption of proteins and other moieties (e.g., sugars, phospholipids, amino acids) occur until equilibrium is reached. However, only certain proteins are able to bind selectively and irreversibly to the implant surface and this is influenced by ions released by bioactive glass, surface morphology, particle size and roughness, as well as protein composition and concentration. For this purpose, the presence of nanometric features on the implant surface may promote the adhesion of proteins involved in the regulation of osteoblast proliferation [36]. At the same time, microscale features stimulate the adhesion and differentiation of the same cells [47]. Therefore, glass-ceramics, with nanoscale crystal sizes and micro-/nanostructured surface topography, show superior bioactivity and promote adhesion, proliferation, osteogenic differentiation of stem cells and osteoblasts and, subsequently, stimulate bone growth [36,37].

Several studies have shown evidence of a strong correlation between substrates' surface morphology and cell adhesion [48], suggesting an enhancement of osteoblasts' adhesion for increasing surface roughness [49]. Therefore, AFM was employed to acquire information on the nanoscale features of the produced bioactive glasses. Figure 4a,b shows two typical $10\ \mu\text{m} \times 10\ \mu\text{m}$ 3D height maps of the 13-93 and 13-93-B3 coated Ti, respectively, highlighting marked differences on nanoscale surface features. In particular, while the 13-93 silicate glass film is characterized by spherical or ellipsoidal

particles of size ranging between 0.2 and 3 μm , the 13-93-B3 borate glass coating shows a lower density of deposited particles, with sizes in the 0.1–1 μm range. The surface roughness evaluated from 10 $\mu\text{m} \times 10 \mu\text{m}$ AFM images and expressed as RMS values (R_q) has values of 186 ± 16 and 52 ± 11 nm for the silicate and borate glasses, respectively. However, these results are strongly affected by the Ti substrates' morphology. In order to highlight the nanometric roughness of the deposited films, 1 $\mu\text{m} \times 1 \mu\text{m}$ images were acquired (Figure 4c,d), resulting in very similar average R_q values for silicate and borate glass coatings (35 ± 12 and 44 ± 18 nm, respectively).

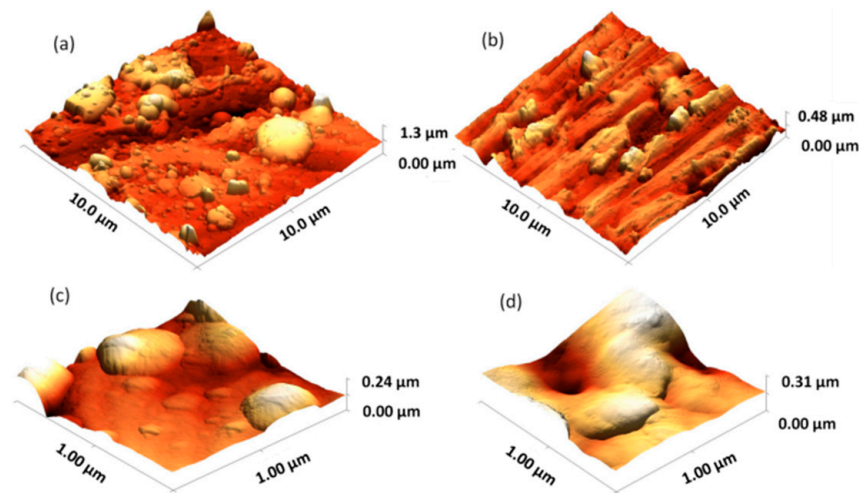


Figure 4. AFM images of (a,c) 13-93 and (b,d) 13-93-B3 BG coated Ti.

3.2. Biological Properties

ADMSCs were employed for the *in vitro* evaluation of cytotoxicity and osteogenic properties of the 13-93 and 13-93-B3 BG coated Ti. Adult adipose tissue of different species has a great potential as source of multipotent cells that are able to differentiate in different lineages [50]. The main advantage of choosing ADMSCs is their abundance and the easy and minimally invasive way to collect them by liposuction, making ADMSCs of great interest in the cell therapy field.

In order to study the cytotoxicity effect of the 13-93 and 13-93-B3 BG coated Ti samples, the MTT assay was performed. ADMSCs were incubated with and without (control sample) the two bioactive glass coatings and then treated with the MTT. The consequent formation of blue formazan crystals is possible only in the cells with metabolic activity. Therefore, the determination by the $\text{OD}_{600 \text{ nm}}$ of formazan is related to the percentage of living cells. The measurements were executed in triplicate after 24 and 48 h of incubation time. The calculated averages are reported in Figure 5. It is possible to assert that both samples are not cytotoxic since no significant differences are noticeable between the samples incubated with 13-93 and 13-93-B3 BG coated Ti and the control sample both at 24 and 48 h of incubation time.

In Figure 6, it is possible to observe the extracellular calcium deposition detected by Alizarin Red stain in ADMSCs, a clear demonstration of the osteogenic differentiation, except for the negative control. No significant differences were detected for the 13-93 and 13-93-B3 coatings, while the percentage of red portion in Figure 6a,b and Figure 6c,d seems to be slightly more than in the positive control sample (Figure 6e,f).

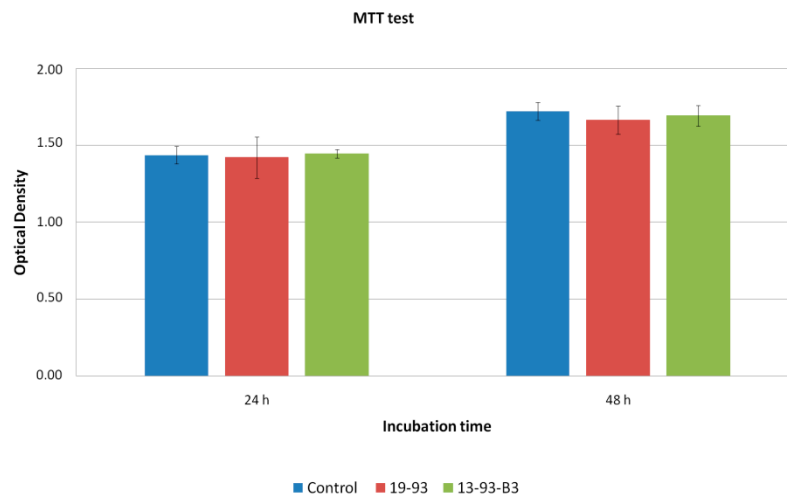


Figure 5. MTT results of 13-93 and 13-93-B3 BG coated Ti after 24 and 48 h of in vitro ADMSC culture, reported as optical density measured at 600 nm, expressed as mean values \pm standard deviation of 3 independent experiments. Statistical analysis was performed through ANOVA, followed by post hoc Tukey test.

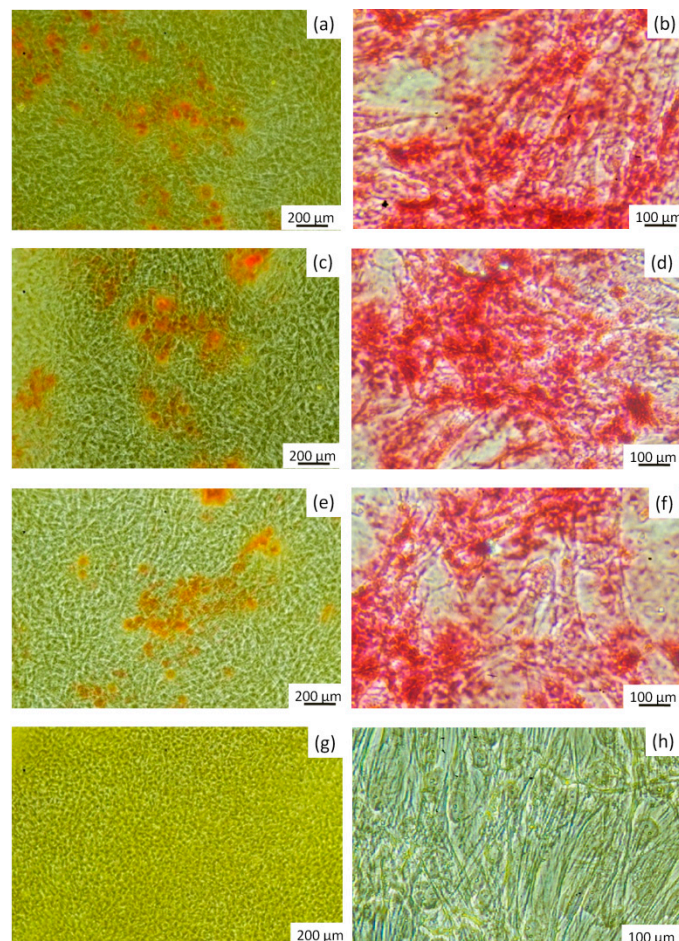


Figure 6. Optical microscopic images taken after staining with Alizarin Red S of ADMSCs cultured in the presence of (a,b) 13-93 BG coated Ti, (c,d) 13-93-B3 BG coated Ti in osteogenic medium, (e,f) positive control and (g,h) negative control (ADMSCs cultured with or without osteogenic medium, respectively) for three weeks. The magnification is 20 \times (on the left) and 40 \times (on the right).

The effect of the 13-93 and 13-93-B3 BG coated Ti on various microorganisms (*E. faecalis*, *E. coli*, *P. aeruginosa*, *S. aureus*) was evaluated after incubation at 37 °C for 24 h. The results of the OD_{600 nm} measured with a BioPhotometer are shown in Figure 7, where the OD values are properly multiplied for the dilution factor. It is possible to note that even if borate glasses should have antibacterial properties, as follows from the literature [28–30], all microbiology tests show a rather high proliferation of all the four tested bacteria strains, comparative or higher than the control sample. In particular, for the Gram+ bacteria *E. faecalis* no significant differences can be noted with respect to the control sample; whereas slight differences can be observed for the Gram+ *S. aureus*. For the Gram– bacteria (*E. coli* and *P. aeruginosa*), their growth is favored by the presence of both the deposited coatings. No antibacterial effects can be expected for silicate glass films and, probably, the absence of these properties also for borate glass films can be imputed to the amount of boron released by the coatings, which could be too low to inhibit bacterial growth. Therefore, if the aim is to deposit thin bioactive films that also present antimicrobial effects, the addition of specific ions in the glass composition, such as Ag, Zn or Cu, is advisable [9,28,30,51].

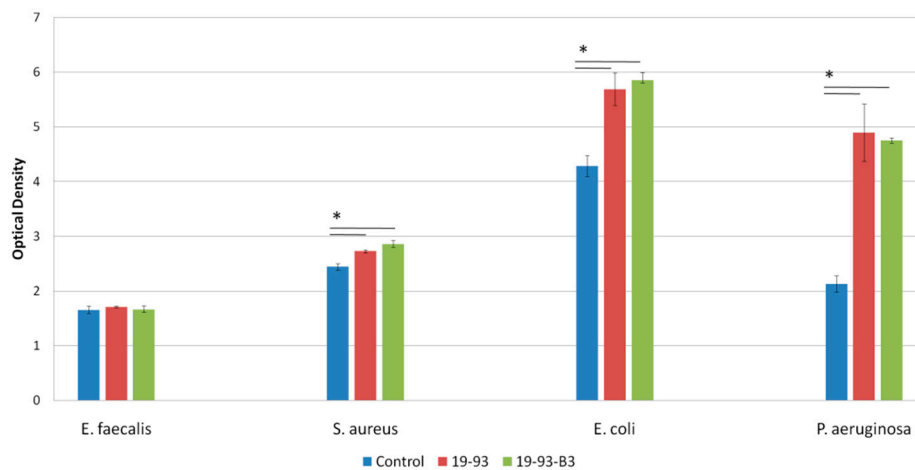


Figure 7. Antibacterial test carried out on 13-93 and 13-93-B3 BG coated Ti compared with the control sample, reported as optical density measured at 600 nm (obtained values are multiplied by the dilution factor), expressed as mean values \pm standard deviation of 3 independent experiments. Statistical analysis was performed through ANOVA, followed by post hoc Tukey test (* $p < 0.05$).

4. Conclusions

Silicate (13-93) and borate (13-93-B3) bioactive glasses were successfully deposited on Ti substrate by ns-Pulsed Laser Deposition. The deposited films, characterized by SEM, AFM and XRD techniques, exhibit similar features: they are a few microns thick, amorphous, compact and crack free, and their morphologies are characterized by the presence of micrometric and nanometric particles. The cytocompatibility of coatings of both glass compositions was demonstrated by the MTT test and their osteogenic differentiation activity was studied after ADMSCs' growth in osteogenic medium and staining with Alizarin Red. Although it was reported that bulk 13-93-B3 can inhibit bacterial growth [28–30], no antibacterial effect of borate (13-93-B3) glass coatings on Ti was detected against the tested bacteria strains *E. faecalis*, *E. coli*, *P. aeruginosa* and *S. aureus*.

The results prove the potential use of the PLD technique to deposit dense, compact and crack-free silicate and borate coatings that retain the biological activity of the bulk materials. Further studies will be focused on the addition of other ions to the glass composition for imparting antibacterial properties to the implant coatings.

Author Contributions: Conceptualization, J.V.R. and A.R.B.; methodology, A.D.B. and R.T.; validation, J.V.R., A.D.B., K.B., R.T., and A.R.B.; investigation, M.C., K.S., K.B., and G.D.B.; resources, J.V.R., A.D.B., K.B., G.D.B., R.T., and A.R.B.; data curation, M.C., K.B., and G.D.B.; writing—original draft, J.V.R., M.C., A.D.B., and K.B.; writing—review and editing, J.V.R., M.C., A.D.B., and K.B. All authors have read and agreed to the published version of the manuscript.

Funding: This research was partially funded by the Italian Ministry of Health, Grant Nos. IZS LT 02/15 RC and IZS LT 01/17 RC.

Acknowledgments: The authors are grateful to Ettore Galvano for support in performing the cell tests. The technical assistance of Luca Imperatori, Massimo Di Menno Di Bucchianico and Marco Orteni is gratefully acknowledged. ÅboAkademi's Johan Gadolin Scholarship, and Leena Hupa, are gratefully acknowledged for a visiting fellowship for K.S.

Conflicts of Interest: The authors declare no conflict of interest.

References

1. Hench, L.L.; Polak, J.M. Third-generation biomedical materials. *Science* **2002**, *295*, 1014–1017. [[CrossRef](#)] [[PubMed](#)]
2. Vallet-Regí, M. Evolution of bioceramics within the field of biomaterials. *C. R. Chim.* **2010**, *13*, 174–185. [[CrossRef](#)]
3. Brånemark, P.I.; Breine, U.; Johansson, B.; Roylance, P.J.; Röckert, H.; Yoffey, J.M. Regeneration of bone marrow. *Cell Tissue Organs* **1964**, *59*, 1–46. [[CrossRef](#)]
4. Rau, J.V.; Teghil, R.; Fosca, M.; De Bonis, A.; Cacciotti, I.; Bianco, A.; Rossi Albertini, V.; Caminiti, R.; Ravaglioli, A. Bioactive glass-ceramic coatings prepared by pulsed laser deposition from RKKP targets (sol-gel vs melt-processing route). *Mater. Res. Bull.* **2012**, *47*, 1130–1137. [[CrossRef](#)]
5. Rau, J.V.; Cacciotti, I.; Laureti, S.; Fosca, M.; Varvaro, G.; Latini, A. Bioactive, nanostructured Si-substituted hydroxyapatite coatings on titanium prepared by pulsed laser deposition. *J. Biomed. Mater. Res. Part B Appl. Biomater.* **2015**, *103 B*, 1621–1631. [[CrossRef](#)]
6. De Bonis, A.; Curcio, M.; Fosca, M.; Cacciotti, I.; Santagata, A.; Teghil, R.; Rau, J.V. RBP1 bioactive glass-ceramic films obtained by pulsed laser deposition. *Mater. Lett.* **2016**, *175*, 195–198. [[CrossRef](#)]
7. Ledda, M.; Fosca, M.; De Bonis, A.; Curcio, M.; Teghil, R.; Lolli, M.G.; De Stefanis, A.; Marchese, R.; Rau, J.V.; Lisi, A. Placenta derived mesenchymal stem cells hosted on RKKP glass-ceramic: A tissue engineering strategy for bone regenerative medicine applications. *BioMed Res. Int.* **2016**, *2016*, 3657906. [[CrossRef](#)]
8. Curcio, M.; De Stefanis, A.; De Bonis, A.; Teghil, R.; Rau, J.V. Pulsed laser deposited bioactive RKKP-Mn glass-ceramic coatings on titanium. *Surf. Coat. Technol.* **2019**, *357*, 122–128. [[CrossRef](#)]
9. Rau, J.V.; Curcio, M.; Raucci, M.G.; Barbaro, K.; Fasolino, I.; Teghil, R.; Ambrosio, L.; De Bonis, A.; Boccaccini, A.R. Cu-releasing bioactive glass coatings and their in vitro properties. *ACS Appl. Mater. Interfaces* **2019**, *11*, 5812–5820. [[CrossRef](#)]
10. Hench, L.L.; Splinter, R.J.; Allen, W.C.; Greenlee, T.K. Bonding mechanisms at the interface of ceramic prosthetic materials. *J. Biomed. Mater. Res. Symp.* **1971**, *2*, 117–141. [[CrossRef](#)]
11. Song, Z.; Borgwardt, L.; Høiby, N.; Wu, H.; Sørensen, T.S.; Borwardt, A. Prosthesis infections after orthopedic joint replacement: The possible role of bacterial biofilms. *Orthop. Rev.* **2013**, *5*, 65–71. [[CrossRef](#)] [[PubMed](#)]
12. Andersson, Ö.H. Glass transition temperatures of glasses in the SiO₂-Na₂O-CaO-P₂O₅-Al₂O₃-B₂O₃ system. *J. Mater. Sci. Mater. Med.* **1992**, *3*, 326–328. [[CrossRef](#)]
13. Brink, M.; Turunen, T.; Happonen, R.P.; Yli-Urpo, A. Compositional dependence of bioactivity of glasses in the system Na₂O-K₂O-MgO-CaO-B₂O₃-P₂O₅-SiO₂. *J. Biomed. Mater. Res.* **1997**, *37*, 114–121. [[CrossRef](#)]
14. Brink, M.; Karlsson, K.H.; Yli-Urpo, A. Novel Bioactive Glasses and Their Use. Patent No. WO 96/21628, 18 July 1996.
15. Yao, A.; Wang, D.; Huang, W.; Fu, Q.; Rahaman, M.N.; Day, D.E. In vitro bioactive characteristics of borate-based glasses with controllable degradation behaviour. *J. Am. Ceram. Soc.* **2007**, *90*, 303–306. [[CrossRef](#)]
16. Fu, Q.; Rahaman, M.N.; Fu, H.; Liu, X. Silicate, borosilicate, and borate bioactive glass scaffolds with controllable degradation rate for bone tissue engineering applications. I. Preparation and in vitro degradation. *J. Biomed. Mater. Res. A* **2010**, *95A*, 164–171. [[CrossRef](#)]

17. Balasubramanian, P.; Grünewald, A.; Detsch, R.; Hupa, L.; Jokic, B.; Tallia, F.; Solanki, A.K.; Jones, J.R.; Boccaccini, A.R. Ion release, hydroxyapatite conversion, and cytotoxicity of boron-containing bioactive glass scaffolds. *Int. J. Appl. Glass Sci.* **2016**, *7*, 206–215. [[CrossRef](#)]
18. Schuhladen, K.; Wang, X.; Hupa, L.; Boccaccini, A.R. Dissolution of borate and borosilicate bioactive glasses and the influence of ion (Zn, Cu) doping in different solutions. *J. Non-Cryst. Solids* **2018**, *502*, 22–34. [[CrossRef](#)]
19. Balasubramanian, P.; Büttner, T.; Miguez Pacheco, V.; Boccaccini, A.R. Boron-containing bioactive glasses in bone and soft tissue engineering. *J. Eur. Ceram. Soc.* **2018**, *38*, 855–869. [[CrossRef](#)]
20. Huang, W.; Day, D.E.; Kittiratanapiboon, K.; Rahaman, M.N. Kinetics and mechanisms of the conversion of silicate (45S5), borate, and borosilicate glasses to hydroxyapatite in dilute phosphate solution. *J. Mater. Sci. Mater. Med.* **2006**, *17*, 583–596. [[CrossRef](#)]
21. Liu, X.; Rahaman, M.N.; Day, D.E. Conversion of melt-derived microfibrinous borate (13-93B3) and silicate (45S5) bioactive glass in a simulated body fluid. *J. Mater. Sci.: Mater. Med.* **2013**, *24*, 583–595. [[CrossRef](#)]
22. Nielsen, F.H. Studies on the relationship between boron and magnesium which possibly affects the formation and maintenance of bones. *Magnes. Trace Elem.* **1990**, *9*, 61–69. [[CrossRef](#)] [[PubMed](#)]
23. Devirian, T.A.; Volpe, S.L. The physiological effects of dietary boron. *Crit. Rev. Food Sci. Nutr.* **2003**, *43*, 219–231. [[CrossRef](#)] [[PubMed](#)]
24. Marion, N.; Liang, W.; Reilly, G.; Day, D.E.; Rahaman, M.N.; Mao, J.J. Bioactive borate glass supports the osteogenic potential of human mesenchymal stem cells. *Mech. Adv. Mater. Struct.* **2005**, *12*, 239–246. [[CrossRef](#)]
25. Thyparambil, N.J.; Gutgesell, L.C.; Hurley, C.C.; Flowers, L.E.; Day, D.E.; Semon, J.A. Adult stem cell response to doped bioactive borate glass. *J. Mater. Sci. Mater. Med.* **2020**, *31*, 13. [[CrossRef](#)] [[PubMed](#)]
26. Haro Durand, L.A.; Vargas, G.E.; Romero, N.M.; Vera-Mesones, R.; Porto-López, J.M.; Boccaccini, A.R.; Zago, M.P.; Baldi, A.; Gorustovich, A. Angiogenic effects of ionic dissolution products released from a boron-doped 45S5 bioactive glass. *J. Mater. Chem. B* **2015**, *3*, 1142–1148. [[CrossRef](#)]
27. Kalmodia, S.; Molla, A.R.; Basu, B. In vitro cellular adhesion and antimicrobial property of SiO₂-MgO-Al₂O₃-K₂O-B₂O₃-F glass ceramic. *J. Mater. Sci. Mater. Med.* **2010**, *21*, 1297–1309. [[CrossRef](#)]
28. Ottomeyer, M.; Mohammadkhan, A.; Day, D.; Westenberg, D. Broad-spectrum antibacterial characteristics of four novel borate-based bioactive glasses. *Adv. Microbiol.* **2016**, *6*, 776–787. [[CrossRef](#)]
29. Rodriguez, O.; Ston, W.; Schemitsch, E.H.; Zalzal, P.; Waldman, S.; Papini, M.; Towler, M.R. Titanium addition influences antibacterial activity of bioactive glass coatings on metallic implants. *Heliyon* **2017**, *3*, e00420. [[CrossRef](#)]
30. Jung, S.; Day, T.; Boone, T.; Buziak, B.; Omar, A. Anti-biofilm activity of two novel, borate based, bioactive glass wound dressings. *Biomed. Glasses* **2019**, *5*, 67–75. [[CrossRef](#)]
31. Fu, Q.; Rahaman, M.N.; Sonny Bal, B.; Bonewald, L.F.; Kuroki, K.; Brown, R.F. Silicate, borosilicate, and borate bioactive glass scaffolds with controllable degradation rate for bone tissue engineering applications. II. In vitro and in vivo biological evaluation. *J. Biomed. Mater. Res. A* **2010**, *95A*, 1172–1179. [[CrossRef](#)]
32. Peddi, L.; Brow, R.K.; Brown, R.F. Bioactive borate glass coatings for titanium alloys. *J. Mater. Sci. Mater. Med.* **2008**, *19*, 3145–3152. [[CrossRef](#)] [[PubMed](#)]
33. Matinmanesh, A.; Li, Y.; Nouhi, A.; Zalzal, P.; Schemitsch, E.H.; Towler, M.R.; Papini, M. Evaluating the critical strain energy release rate of bioactive glass coatings on Ti₆Al₄V substrates after degradation. *J. Mech. Behav. Biomed. Mater.* **2018**, *78*, 273–281. [[CrossRef](#)] [[PubMed](#)]
34. Kargozar, S.; Montazerian, M.; Fiume, E.; Bano, F. Multiple and promising applications of strontium (Sr)-containing bioactive glasses in bone tissue engineering. *Front. Bioeng. Biotechnol.* **2019**, *7*, 161. [[CrossRef](#)] [[PubMed](#)]
35. Rau, J.V.; Antoniac, I.; Fosca, M.; De Bonis, A.; Blajan, A.I.; Cotrut, C.; Graziani, V.; Curcio, M.; Cricenti, A.; Niculescu, M.; et al. Glass-ceramic coated Mg-Ca alloys for biomedical implant applications. *Mater. Sci. Eng. C* **2016**, *64*, 362–369. [[CrossRef](#)]
36. Gittens, R.A.; Mclachlan, T.; Olivares-Navarrete, R.; Cai, Y.; Berner, S.; Tannenbaum, R.; Schwartz, Z.; Sandhage, K.H.; Boyan, B.D. Biomaterials the effects of combined micron-/submicron-scale surface roughness and nanoscale features on cell proliferation and differentiation. *Biomaterials* **2011**, *32*, 3395–3403. [[CrossRef](#)]
37. Im, B.J.; Lee, S.W.; Oh, N.; Lee, M.H.; Kang, J.H.; Leesungbok, R.; Lee, S.C.; Ahn, S.J.; Park, J.S. Texture direction of combined microgrooves and submicroscale topographies of titanium substrata influence adhesion, proliferation, and differentiation in human primary cells. *Arch. Oral Biol.* **2011**, *57*, 898–905. [[CrossRef](#)]

38. Ma, J.; Wang, C.Z.; Ban, C.L.; Chen, C.Z.; Zhang, H.M. Pulsed laser deposition of magnesium-containing bioactive glass film on porous Ti-6Al-4V substrate pretreated by micro-arc oxidation. *Vacuum* **2016**, *125*, 48–55. [[CrossRef](#)]
39. Sanz, C.K.; dos Santos, A.R.; da Silva, M.H.P.; Marçal, R.; Tute, E.M.; Meza, E.L.; Mello, A.; Borghi, F.F.; de Souza Camargo, S.A. Niobo-phosphate bioactive glass films produced by pulsed laser deposition on titanium surfaces for improved cell adhesion. *Ceram. Int.* **2019**, *45*, 18052–18058. [[CrossRef](#)]
40. Shaikh, S.; Shaikh, S.; Majumdar, A.G.; Subramanian, M.; Sucharita, S. 45S5 bioactive glass coating on Ti6Al4V alloy using pulsed laser deposition technique. *Mater. Res. Express* **2020**, *6*, 125428. [[CrossRef](#)]
41. Wang, D.G.; Zhang, W.L.; Li, H.J.; Zhang, J.H.; Chen, C.Z. HA/BG composite films deposited by pulse laser under O₂ atmosphere. *Ceram. Int.* **2017**, *43A*, 672–676. [[CrossRef](#)]
42. Wang, D.G.; Chen, C.Z.; Yang, X.X.; Ming, X.C.; Zhang, W.L. Effect of bioglass addition on the properties of HA/BG composite films fabricated by pulsed laser deposition. *Ceram. Int.* **2018**, *44*, 14528–14533. [[CrossRef](#)]
43. Abdelghany, A.M.; Elbatal, H.A.; Ezzeldin, F.M. Bone bonding ability behavior of some ternary borate glasses by immersion in sodium phosphate solution. *Ceram. Int.* **2012**, *38*, 1105–1113. [[CrossRef](#)]
44. Gyorgy, E.; Grigorescu, S.; Socol, G.; Mihailescu, I.N.; Janackovic, D.; Dindune, A.; Kanepe, Z.; Palcevskis, E.; Zdrentu, E.L.; Petrescu, S.M. Bioactive glass and hydroxyapatite thin films obtained by pulsed laser deposition. *Appl. Surf. Sci.* **2007**, *253*, 7981–7986. [[CrossRef](#)]
45. Liste, S.; Serra, J.; González, P.; Borrajo, J.P.; Chiussi, S.; León, B.; Pérez-Amor, M. The role of the reactive atmosphere in pulsed laser deposition of bioactive glass films. *Thin Solid Films* **2004**, *453–454*, 224–228. [[CrossRef](#)]
46. Lefebvre, L.; Chevalier, J.; Gremillard, L.; Zenati, R.; Thollet, G.; Bernache-Assolant, D.; Govin, A. Structural transformations of bioactive glass 45S5 with thermal treatments. *Acta Mater.* **2007**, *55*, 3305–3313. [[CrossRef](#)]
47. Begam, H.; Kundu, B.; Chanda, A.; Nandi, S. MG63 osteoblast cell response on Zn doped hydroxyapatite (HAp) with various surface features. *Ceram. Int.* **2017**, *43*, 3752–3760. [[CrossRef](#)]
48. Donoso, N.G.; Mendez-Vilas, A.; Bruque, J.M.; Gonzalez-Martin, M.L. On the relationship between common amplitude surface roughness parameters and surface area: Implications for the study of cell–material interactions. *Int. Biodeterior. Biodegrad.* **2007**, *59*, 245–251. [[CrossRef](#)]
49. Zareidoost, A.; Yousefpour, M.; Ghaseme, B.; Amanzadeh, A. The relationship of surface roughness and cell response of chemical surface modification of titanium. *J. Mater. Sci. Mater. Med.* **2012**, *23*, 1479–1488. [[CrossRef](#)]
50. Alipour, F.; Parham, A.; KazemiMehrerjerd, H.; Dehghani, H. Equine adipose-derived mesenchymal stem cells: Phenotype and growth characteristics, gene expression profile and differentiation potentials. *Cell J.* **2015**, *16*, 456–465.
51. Ciraldo, F.E.; Liverani, L.; Gritsch, L.; Goldmann, W.H.; Boccaccini, A.R. Synthesis and characterization of silver-doped mesoporous bioactive glass and its applications in conjunction with electrospinning. *Materials* **2018**, *11*, 692. [[CrossRef](#)]

Publisher’s Note: MDPI stays neutral with regard to jurisdictional claims in published maps and institutional affiliations.



© 2020 by the authors. Licensee MDPI, Basel, Switzerland. This article is an open access article distributed under the terms and conditions of the Creative Commons Attribution (CC BY) license (<http://creativecommons.org/licenses/by/4.0/>).